

Modified Gravity Spins Up Galactic Halos

Jounghun Lee¹, Gong-Bo Zhao^{2,3}, Baojiu Li⁴ and Kazuya Koyama²

ABSTRACT

We investigate the effect of modified gravity on the specific angular momentum of galactic halos by analyzing the halo catalogs at $z = 0$ from high-resolution N -body simulations for a $f(R)$ gravity model that meets the solar-system constraint. It is shown that the galactic halos in the $f(R)$ gravity model tend to acquire significantly higher specific angular momentum than those in the standard Λ CDM model. The largest difference in the specific angular momentum distribution between these two models occurs for the case of the isolated galactic halos with mass less than $10^{11} h^{-1} M_{\odot}$, which are likely least shielded by the chameleon screening mechanism. As the specific angular momentum of galactic halos is rather insensitive to the other cosmological parameters, it can in principle be an independent discriminator of modified gravity. We speculate a possibility of using the relative abundance of the low surface brightness galaxies (LSBGs) as a test of GR given that the formation of the LSBGs befalls in the fast spinning dark halos.

Subject headings: cosmology:theory — methods:statistical — large-scale structure of universe

1. INTRODUCTION

It has been almost one century since Einstein introduced his theory of general relativity (GR) as a mathematical framework within which the evolution of the Universe can be coherently described. Remarkably successful as it has been as a foundation of modern cosmology,

¹Astronomy Program, Department of Physics and Astronomy, FPRD, Seoul National University, Seoul 151-747, Korea; jounghun@astro.snu.ac.kr

²Institute of Cosmology & Gravitation, University of Portsmouth, Portsmouth, PO1 3FX, UK

³National Astronomy Observatories, Chinese Academy of Science, Beijing, 100012, P.R.China

⁴Institute of Computational Cosmology, Department of Physics, Durham University, Durham DH1 3LE, UK

the triumph of GR is contingent upon one crucial caveat that the Universe is dominantly filled with an exotic energy component with negative pressure (dubbed *dark energy*) which is believed to accelerate the Universe at present epoch (Riess et al. 1998; Perlmutter et al. 1999). Although the cosmological constant Λ devised by Einstein himself is currently the paradigm of dark energy, the extreme fine-tuning of Λ required to explain the observations has provoked skepticism among the cosmologists about the validity of the standard Λ CDM cosmology (Λ +cold dark matter) based on GR.

Recently, a flurry of research has been conducted on modified gravity (MG) models, which attempt to modify GR on large scales so that the apparent acceleration of the Universe can be realized without introducing dark energy (see Clifton et al. 2012, for a recent review). Among many different MG models that have been put forward so far, the $f(R)$ gravity (Sotiriou & Faraoni 2010; de Felice & Tsujikawa 2010) has attracted even more attentions after the recent stringent observational tests (Reyes et al. 2010; Wojtak et al. 2011). Basically, the $f(R)$ gravity generalizes the Ricci scalar R in the Einstein-Hilbert action for GR to a specific function of R , which gives rise to an extra scalar degree of freedom $f_R \equiv df/dR$, dubbed *scalaron* (Sotiriou & Faraoni 2010; de Felice & Tsujikawa 2010).

The scalaron produces an additional fifth force that modifies GR on large scales. In highly dense environments, however, due to the chameleon mechanism that effectively shields the fifth force, GR is recovered (Khoury & Weltman 2004; Li & Barrow 2007). For a given functional form of $f(R)$, the formation of the cosmic structures and its clustering strength is determined by the magnitude of scalaron at the present epoch, $|f_{R0}|$. The Λ CDM cosmology based on GR corresponds to the case of $f_{R0} = 0$, i.e., $f(R) = \Lambda$. The non-zero value of f_{R0} that is the essential feature of $f(R)$ gravity, however, should be small enough to meet the observational constraints.

Throughout this Paper, we will focus on the Hu-Sawicki $f(R)$ gravity which has the following functional form (Hu & Sawicki 2007)

$$f(R) = -m^2 \frac{c_1(-R/m^2)^n}{c_2(-R/m^2)^n + 1}, \quad (1)$$

with two characteristic parameters of n and c_1/c_2 . Here, $m \equiv 8\pi G\bar{\rho}_m/3$ with mean matter density $\bar{\rho}_m$ at present epoch, and the free parameter c_1/c_2 is related to the Λ density (Ω_Λ) and matter density (Ω_m) parameters as $c_1/c_2 = 6\Omega_\Lambda/\Omega_m$ which mimics the evolution of the Λ CDM background. Regarding the other free parameter, n , we set its value at unity as in the previous works (Oyaizu 2008; Zhao et al. 2011).

The observed abundance of galaxy clusters has constrained the present value of the scalaron in the Hu-Sawicki model to be $|f_{R0}| \lesssim 10^{-4}$ (Schmidt et al. 2009; Lombriser et al.

2010), while the solar system test puts a more stringent constraint of $|f_{R0}| \lesssim 10^{-6}$ for the Milky way halo (Hu & Sawicki 2007). When the scalaron meets this constraint, however, it is very difficult to distinguish the $f(R)$ gravity model from the Λ CDM model based on GR since there is very little difference between the two models in their predictions for almost all observables.

Here we suggest that it might be possible to discriminate $f(R)$ gravity from GR by measuring the specific angular momentum distribution of the low-mass galactic halos located in low-density environments (i.e., the field regions) where the chameleon mechanism functions less effectively. We expect that due to the effect of the fifth force of the scalaron the low-mass field galactic halos in the $f(R)$ gravity case would acquire higher specific angular momentum than those in the GR case. Whereas, the galactic halos located in high-density environments where the chameleon shielding mechanism effectively screens the fifth force would not show any difference in the specific angular momentum distribution between the two models (Zhao et al. 2011; Li et al. 2012a).

Note that the expected enhancement in the specific angular momentum of the low-mass field galactic halos is essentially the same effect of the fifth force that enhances the velocity dispersion of unscreened halos, which was first discussed by Schmidt (2010) and also by Zhao et al. (2011). The main difference is that for the case of the angular momentum what takes into account is only the velocity components perpendicular to the separation from the halo center on which the gravity act as a tidal torque forces. The enhanced gravity due to the presence of the fifth force leads to the enhanced tidal torque forces which in turn induces higher angular momentum of an unscreened halo.

To investigate quantitatively how significantly the distribution of the specific angular momentum differs between the GR and the $f(R)$ gravity cases, we use the high-resolution N-body simulations for the two models to determine the distributions of the specific angular momentum of the low-mass field galactic halos. Being conservative, we consider the case of $|f_{R0}| = 10^{-6}$ as our fiducial $f(R)$ gravity model, calling it “F6 model” from here on. The contents of this Paper are outlined as follows. In section 2 we describe the numerical data from the N-body simulations and present the results on the specific angular momentum and spin parameter distributions of the low-mass field galactic halos for the GR and the F6 cases. In section 3 we speculate a possibility of using the abundance of the low surface brightness galaxies as a probe of modified gravity. In section 4 we discuss the results and draw a final conclusion.

2. TIDAL EFFECT OF THE F(R) GRAVITY

2.1. Numerical data

We have performed high-resolution N -body simulations which implement the ECOS-MOG code (Li et al. 2012b) to compute the trajectories of 512^3 dark matter particles in a periodic box of size $100 h^{-1}\text{Mpc}$ on a side for the GR and F6 models. The key cosmological parameters that describe the initial conditions of each model are identically set at the WMAP7 values ($\Omega_m = 0.24$, $\Omega_\Lambda = 0.76$, $\Omega_b = 0.045$, $h = 0.73$, $\sigma_8 = 0.77$, $n_s = 0.96$) (Komatsu et al. 2011). The bound dark matter halos are identified from the simulation data by applying the AHF (Amiga’s Halo Finder) code (Knollmann & Knebe 2009) which defines the halo mass M as the top-hat mass enclosed by the spherical radius R at which the overdensity reaches the threshold value of $\Delta_v = 374$ at $z = 0$. For the details of the simulations and the halo-identification procedures, see Knollmann & Knebe (2009) and Li et al. (2012a,b).

Among the identified halos for each model, we select only those well resolved halos which consist of 100 or more dark matter particles ($N_p \geq 100$). Then, we measure the physical angular momentum, \mathbf{J} , of each selected halo as $\mathbf{J} = \sum_i^{N_p} m_i \mathbf{v}_i \times \mathbf{r}_i$ where m_i , \mathbf{v}_i and \mathbf{r}_i represent the mass, velocity and position of the i -th particle belonging to the halo. Here the positions of the component particles, $\{\mathbf{r}_i\}_1^{N_p}$, are all measured with respect to the center of mass of their host halo. We divide the selected halos into the *field* halos and the *wall* halos by applying the friends-of-friends (FoF) criterion which has been conventionally used in observational data analysis for the separation between the field and the wall galaxies. The usefulness of the FoF criterion lies in the fact that it requires no other information than the positions of the sample galaxies and thus that it can be readily applied to real observational data in practice. Very recently, Zhao et al. (2011) and Cabré et al. (2012) have developed more elaborate criteria with which the screened and unscreened halos can be separated. However, in the current work, we choose the simple FoF criterion for the practical purpose.

We first measure the mean separation distance $\bar{\ell}$ among the selected halos, and then classify those isolated halos which do not have any neighboring halos within the threshold distance of $b\bar{\ell}$ as field halos, where b is the linkage length parameter. The rest of the selected halos are classified as wall halos which have at least one neighboring halo within $b\bar{\ell}$, residing in relatively higher density regions. The larger the value of b is, the more isolated the field galactic halos are. Here, we set the linkage length parameter at $b = 0.2$. We also restrict our analysis to the *galactic* halos which are less massive than a given mass threshold M_c for which we consider two cases of $M_c = 10^{11}$ and $10^{12} h^{-1} M_\odot$. In Table 1 we list the total number of the well-resolved halos with $N_p \geq 100$ (N_{total}), the mean halo separation $\bar{\ell}$, the

numbers of the field galactic halos for two different mass thresholds.

2.2. Distribution of the Specific Angular Momentum

The specific angular momentum, \mathbf{j} , of each field (wall) galactic halo is computed as $\mathbf{j} \equiv \mathbf{J}/M$, in unit of $[s^{-1}\text{km } h^{-1}\text{Mpc}]$. Binning the magnitude of the specific angular momentum, j , and counting the number ΔN_g , of the field (wall) galactic halos which belong to each j -bin, we determine the probability density distribution of the specific angular momentum of the field (wall) galactic halos as $p(j) = \Delta N_g / (N_g \Delta j)$, where N_g is the total number of the field (wall) galactic halos and Δj represents the size of each j -bin.

Figure 1 shows the probability density distributions, $p(j)$, of the field and wall galactic halos with the Jack-knife errors for two different cases of M_c in four separate panels. We construct eight Jack-knife resamples of equal size and then calculated σ_j as one standard deviation scatter of $p(j)$ among the eight resamples. In each panel the solid and dashed lines represent the result for the GR and F6 cases, respectively. As can be seen, the galactic halos in the F6 model have higher specific angular momentum than those in GR. Furthermore, the field galactic halos with lower mass of $M \leq 10^{11} h^{-1} M_\odot$ exhibit the largest difference between the two models. We interpret this result as follows. The enhanced gravity in the F6 model exerts enhanced tidal torque forces on the proto-galaxies in the field regions, and in consequence the field galactic halos for the F6 case to acquire higher specific angular momentum than for the GR case.

To test the null hypothesis that there is no difference in the distribution of the specific angular momentum of the low-mass field galactic halos between the GR and the F6 cases, we perform the two-sample KS (Kolmogorov-Smirnov) test (Wall & Jenkins 2003). Figure 2 shows the cumulative fraction function of the specific angular momentum of the low-mass field galactic halos ($M \leq 10^{11} h^{-1} M_\odot$) for the GR (solid line) and F6 (dashed line) cases. Measuring the KS statistic, i.e., the maximum distance between the two cumulative fraction functions is found to be 203, which rejects the null hypothesis at 99.9999% confidence level.

Now that the difference in the distribution of j of the low-mass field galactic halos between the GR and F6 cases is found to be statistically significant, it is important to see whether the two cases have comparable mass distributions. For this, we first calculate the following three quantities: First, the probability density distribution of the logarithmic mass of the field galactic halos as $p(\ln M) \equiv \Delta N_g / (N_g \Delta \ln M)$, where N_g is the total number of the field galactic halos, ΔN_g is the number of the field galactic halos belonging to each logarithmic mass bin and $\Delta \ln M$ is the size of the logarithmic mass bin. Second, the number

densities of the field galactic halos per unit volume, $dN/d\ln M \equiv \Delta N_g/(V\Delta\ln M)$ in unit of $h^3\text{Mpc}^{-3}$, where V represents the volume of the simulation box. Third, the mean mass of the field galactic halos belonging to each logarithmic mass bin, $\langle M \rangle \equiv \Delta M/\Delta N_g$, where ΔM represents the sum of the masses of the field galactic halos belonging to each logarithmic mass bin.

Figure 3 shows $p(\ln M)$ and $dN/d\ln M$ in the bottom and top panels, respectively. In each panel the solid and dashed lines represent the GR and F6 cases, respectively. As can be seen, although the F6 model yields $\sim 10\%$ increment in the amplitude of the mass function of the field galactic halos, $p(\ln M)$ in the two models are almost identical to each other. Figure 4 shows the ratio of $\langle M \rangle$ for the F6 case to that for the GR case, which reveals that the difference in the mean mass between the two models is less than 1% in the whole mass range of the field galactic halos. The results shown in Figures 3-4 prove that the two samples are comparable in the mass distribution and thus that the difference in j between the two models are not due to the mass-bias.

To test if the difference in $p(j)$ of the low-mass galactic halos between the GR and F6 models shown in Figure 1 is really due to the effect of the fifth force but not due to any possible numerical flukes, we multiply the factor of $(4/3)^{1/2}$ to the values of j of the low-mass field galactic halos for the GR case and determine its probability density distribution, $p[(4/3)^{1/2}j]$. The gravitational tidal force in the low-density regions can be enhanced by a maximum factor of $4/3$ for the F6 case. That is, the low-mass field galactic halos at their proto-galactic stages would experience enhanced gravitational tidal force in the F6 model. In consequence, the velocities that enter in the definition of the specific angular momentum would increase by a maximum factor of $(4/3)^{1/2}$, which in turn leads to the enhanced specific angular momentum of the low-mass field galactic halos by the same factor. Therefore, it is expected that $p_{GR}[(4/3)^{1/2}j]$ should match the probability density distribution of j of the low-mass field galactic halos for the F6 case, $p_{F6}(j)$.

Figure 5 shows $p_{GR}[(4/3)^{1/2}j]$ (dotted line) and compares it with $p_{F6}(j)$ (dashed line). As can be seen, the two distributions agree with each other very well, which confirms that the difference in $p(j)$ of the low-mass field galactic halos is due to the effect of modified gravity which can be enhanced by a maximum factor of $4/3$ in the low-density environments. This result is also consistent with the previous works of Schmidt (2010) and Zhao et al. (2011) who showed that the effect of MG enhances the velocity dispersion of a unscreened halo by a factor of $(4/3)^{1/2}$. The fact that the measurements of the velocity dispersion and the specific angular momentum yield an enhancement of the same factor for unscreened halos indicates that the velocity structure is unchanged by the modified forces at first order.

Figure 6 shows the ratio of $p(j)$ of the wall galactic halos to that of the field galactic

halos, $p_{\text{wall}}(j)/p_{\text{field}}(j)$, for the GR and F6 cases. As can be seen, for GR, the ratio increases rapidly with j , while for the F6 case the rate of the increase of the ratio with j is much milder. The dominance of wall galactic halos in the high- j section is attributed to frequent merger events in high-density regions. As the merging rate is much lower in the field regions for the GR case, it is natural to expect that most of the field galactic halos are biased toward the low j section. In contrast, for the F6 case, even though frequent merging events do not occur in the low-density regions, the unscreened fifth force has an effect of spinning up the field galactic halos, resulting in the increase of the relative abundance of the high- j field galactic halos and the decrease of $p_{\text{wall}}(j)/p_{\text{field}}(j)$ at the high- j end.

One may also expect that the more field galactic halos would acquire on average stronger effect of the enhanced gravitational tidal force since the degree of the chameleon effect is lower in the more field regions. To investigate how the probability density distribution, $p(j)$, depends on the degree of the isolation of the field galactic halos, we calculate $p(j)$ repeatedly, varying the value of b from 0.1 to 0.3. Figure 7 shows the ratio of $p(j)$ of the field galactic halos for the F6 case to that for the GR case, $p_{\text{F6}}(j)/p_{\text{GR}}(j)$, for three different cases of the linkage parameter b . As can be seen, the larger the value of b is, the larger the ratio, $p_{\text{F6}}(j)/p_{\text{GR}}(j)$ is in the high- j section. This result is consistent with the picture that the chameleon screening of $f(R)$ gravity becomes less effective in low-density regions.

2.3. Distribution of the spin parameter

The specific angular momentum of a galactic halo is commonly expressed in terms of the dimensionless spin parameter (Peebles 1969), which is efficiently defined as $\lambda \equiv j/(2GMR)^{1/2}$ (Bullock et al. 2001, and references therein). N-body simulations found that the probability density distribution of this dimensionless spin parameter is well approximated by the following log-normal distribution (e.g., Barnes & Efstathiou 1987; Bullock et al. 2001):

$$p(\lambda) = \frac{1}{\lambda\sqrt{2\pi}\sigma_\lambda} \exp \left[-\frac{\ln^2(\lambda/\lambda_0)}{2\sigma_\lambda^2} \right]. \quad (2)$$

with $\lambda_0 \approx 0.03$ and $\sigma_\lambda \approx 0.5$. N-body simulations also revealed that the shape of $p(\lambda)$ is almost independent of the initial conditions of the Universe, always following the log-normal form with the same values of λ_0 and σ_λ (Barnes & Efstathiou 1987; Steinmetz & Bartelmann 1995). Furthermore, recent observations also showed that the spin parameters of the observed galaxies seem to be only very weakly correlated with the other physical properties of the galaxies such as overdensity, mass, shape and internal structure (Disney et al. 2008).

For each field galactic halo from our simulation, we compute the spin parameter and calculate the probability density distribution, $p(\lambda)$, for the case of the field galactic halos

with $M \leq 10^{11} h^{-1} M_{\odot}$. Fitting the numerically obtained spin parameter distribution, $p(\lambda)$, of the field galactic halos to Equation (2), we determine the best-fit values of λ_0 and σ_{λ} for both of the GR and F6 cases. Figure 8 shows $p(\lambda)$ (square and circular dots) with the Jackknife errors and compares them with the best-fit log-normal distributions (solid and dashed lines) for the GR and F6 cases, respectively, in the top panel. As can be seen, $p(\lambda)$ is indeed well approximated by the log-normal distribution for both of the cases. Table 2 lists the best-fit values of λ_0 and σ_{λ} for the two models. As can be read, for the GR case, the best-fit values of $\lambda_0 \approx 0.03$ and $\sigma_{\lambda} \approx 0.5$ are consistent with the previous N-body results (Bullock et al. 2001), while the F6 case yields larger values of λ_0 and σ_{λ} as expected.

Our result for the GR case confirms the claim of the previous works that the spin parameter distribution is insensitive to the halo mass scale, surrounding overdensity, and the background cosmology. Note that even though we have considered only the field galactic halos with mass less than $10^{11} h^{-1} M_{\odot}$ from a N-body simulation for a WMAP7 cosmology, we have obtained the log-normal distribution of $p(\lambda)$ with $\lambda_0 \approx 0.03$ and $\sigma_{\lambda} \approx 0.5$ which is identical to the result of Bullock et al. (2001) who used all dark matter halos from a N-body simulation with different cosmological parameters to derive $p(\lambda)$.

Now that $p(\lambda)$ is found to differ significantly between the GR and F6 cases while it is insensitive to the background cosmology, the spin parameter distribution of the low-mass field galactic halos should be a sensitive indicator of underlying gravity. The bottom panel of Fig. 8 shows the ratio of the probability density distribution of λ for the F6 case to that for GR, $p_{\text{F6}}(\lambda)/p_{\text{GR}}(\lambda)$. As can be seen, the ratio exceeds unity at $\lambda \approx 0.05$ and increases sharply in the high- λ section ($\lambda \geq 0.05$). The cumulative probability of $P(\lambda \geq 0.05)$ are found to be 0.22 and 0.31 for the GR and F6 cases, respectively.

3. IMPLICATION ON THE LOW-SURFACE BRIGHTNESS GALAXIES

The results presented in section 2.3 has an interesting possible implication on the abundance of the low surface brightness galaxies (LSBGs) whose apparent fluxes are an order of magnitude lower than the night sky. The LSBGs have been found to occupy a significant fraction ($\sim 30 - 50\%$) of the total field galaxy population (Impey & Bothun 1997, and references therein). Very recently, Geller et al. (2012) determined the galaxy luminosity function, using a magnitude limited sample of the galaxies with R -band magnitude less than 20.6 from the Smithsonian Hectospec Lensing Survey (SHELS) which is a dense redshift survey covering a four degree square region at redshifts $0.02 \leq z < 0.1$. They found that the slope of the luminosity function in the faint-end increases up to 15.2 from 13.2 when the LSB drawf galaxies in the field are included.

Regarding the origin of the LSBGs, several theoretical studies suggested a hypothesis that the only difference of the LSBGs from the ordinary galaxies is their biased formation in the fast-spinning dark halos with $\lambda \geq 0.05$ (Impey & Bothun 1997, and references therein). The faster spinning motion of a host halo results in the decrements of the surface density of its disk galaxy, which in turn is directly proportional to the surface brightness. To test this hypothesis, Jimenez et al. (1998) constructed a theoretical model under the assumption that the dark halos where the LSBGs reside have relatively higher specific angular momentum with the spin parameters larger than 0.05, and compared the predictions of their model with the observed properties of the LSBGs. According to their results, the theoretically predicted properties of the LSBGs such as colors, metallicity and spectra are all in excellent agreements with the observed values. The results of Jimenez et al. (1998) have been confirmed by the follow-up works (Boissier & Prantzos 2000, 2001; Boissier et al. 2003).

Now that the LSBGs are found to occupy a significant fraction of the field galaxy population (over 30%) and located in the fast-spinning dark halos, a fundamental question is whether or not the standard Λ CDM cosmology can produce such abundant fast-spinning dark halos in the field regions. At face values, our results then imply that MG, if existent, would produce more LSBGs in the field regions. The difference between the relative abundances of the LSBGs in the GR and F6 cases (22% and 31%, respectively) is definitely significant even though the F6 model is very similar to GR in its predictions for most other observables.

Besides, it has been known that the spin parameters of dark matter halos depend only very weakly on the initial conditions of the Universe. For instance, Barnes & Efstathiou (1987) have shown by N-body simulations that the spin parameters of dark halos are uncorrelated with the initial overdensities. Steinmetz & Bartelmann (1995) have also found through N-body simulations that there is very weak correlation between the spin parameter λ and the initial rms density fluctuation σ , concluding that the spin parameters should be independent of the type of the initial power spectrum. Recently, Disney et al. (2008) have found by analyzing the observational data that the spin parameters of the local disk galaxies are uncorrelated with the other physical properties of them.

Given our result that the F6 model yields more dark halos with $\lambda \geq 0.05$ and the previous results that the spin parameter is almost independent of the initial conditions of the Universe, the relative fraction of the LSBGs that are believed to reside in halos with $\lambda \geq 0.05$ could be an optimal indicator of the effect of MG.

4. SUMMARY AND CONCLUSION

Analyzing the numerical data from the high-resolution N-body simulations for the Hu-Sawicki $f(R)$ gravity with $|f_{R0}| = 10^{-6}$ (F6 model), we have shown that the probability density distribution, $p(j)$, of the specific angular momentum of the low-mass field galactic halos with $M \leq 10^{11} h^{-1} M_{\odot}$ in the F6 model is significantly shifted toward the higher j section than in the GR case. The null hypothesis that there is no difference in $p(j)$ between the GR and the F6 models is rejected via the KS test at the 99.999% confidence level.

We have also determined from the numerical data the probability density distributions of the dimensionless spin parameter, $p(\lambda)$, for the GR and the F6 models and found that the high-spin field galactic halos with $\lambda \geq 0.05$ occupy 21% and 31% of the total field galactic halo populations for the GR and the F6 models, respectively. Given this result and under the assumption that the host halos of the low-surface brightness galaxies (LSBGs) have spin parameters larger than 0.05, we speculate a possibility of discriminating the $f(R)$ gravity from the GR with the relative abundance of the LSBGs in the field regions.

In order to use the LSBGs as a test of gravity, however, it will be first necessary to assess the possible systematic involved in modeling the surface brightness of the disk galaxies. Recently, Davis et al. (2012) recently claimed that the dwarf void galaxies could be significantly brighter in MG models with chameleon mechanism since the unscreened MG in void regions would play a role of enhancing the intrinsic luminosity of the main sequence stars. The situation could be subtle when other factors are taken into account. For example, the unscreened MG would not only brighten up the stars, but also change the dynamical properties of the host halos. These effects need to be taken into account to relate our predictions for dark matter halos to the abundance of the LSBGs. We plan to work on this issue and hope to report the result elsewhere in the near future.

We thank an anonymous referee for helpful comments. JL acknowledges the support by the National Research Foundation of Korea (NRF) grant funded by the Korea government (MEST, No.2012-0004916) and from the National Research Foundation of Korea to the Center for Galaxy Evolution Research. GBZ and KK are supported by STFC grant ST/H002774/1. BL is supported by the Royal Astronomical Society and Durham University. KK acknowledges supports from the ERC and the Leverhulme trust. A part of numerical computations was done on the Sciama HighPerformance Compute (HPC) cluster which is supported by the ICG, SEPNet and the University of Portsmouth.

REFERENCES

- Barnes, J., & Efstathiou, G. 1987, *ApJ*, 319, 575
- Boissier, S., & Prantzos, N. 2000, *MNRAS*, 312, 398
- Boissier, S., & Prantzos, N. 2001, *MNRAS*, 325, 321
- Boissier, S., Monnier Ragaigne, D., Prantzos, N., et al. 2003, *MNRAS*, 343, 653
- Bullock, J. S., Dekel, A., Kolatt, T. S., et al. 2001, *ApJ*, 555, 240
- Cabré, A., Vikram, V., Zhao, G.-B., Jain, B., & Koyama, K. 2012, *JCAP*, 7, 34
- Clifton, T., Ferreira, P. G., Padilla, A., & Skordis, C. 2012, *Phys. Rep.*, 513, 1
- Dalcanton, J. J., Spergel, D. N., & Summers, F. J. 1997, *ApJ*, 482, 659
- Davis, A.-C., Lim, E. A., Sakstein, J., & Shaw, D. J. 2012, *Phys. Rev. D*, 85, 123006
- Disney, M. J., Romano, J. D., Garcia-Appadoo, D. A., et al. 2008, *Nature*, 455, 1082
- de Felice, A., & Tsujikawa, S. 2010, *Living Reviews in Relativity*, 13, 3
- Geller, M. J., Diaferio, A., Kurtz, M. J., Dell’Antonio, I. P., & Fabricant, D. G. 2012, *AJ*, 143, 102
- Hu, W., & Sawicki, I. 2007, *Phys. Rev. D*, 76, 064004
- Impey, C., & Bothun, G. 1997, *ARA&A*, 35, 267
- Jimenez, R., Heavens, A. F., Hawkins, M. R. S., & Padoan, P. 1997, *MNRAS*, 292, L5
- Jimenez, R., Padoan, P., Matteucci, F., & Heavens, A. F. 1998, *MNRAS*, 299, 123
- Khoury, J., & Weltman, A. 2004, *Phys. Rev. D*, 69, 044026
- Knollmann, S. R., & Knebe, A. 2009, *ApJS*, 182, 608
- Komatsu, E., et al. 2011, *ApJS*, 192, 18
- Li, B., & Barrow, J. D. 2007, *Phys. Rev. D*, 75, 084010
- Li, B., Zhao, G.-B., & Koyama, K. 2012, *MNRAS*, 421, 3481
- Li, B., Zhao, G.-B., Teyssier, R., & Koyama, K. 2012, *JCAP*, 1, 51

- Lombriser, L., Slosar, A., Seljak, U., & Hu, W. 2010, arXiv:1003.300
- Mo, H. J., Mao, S., & White, S. D. M. 1998, MNRAS, 295, 319
- Oyaizu, H. 2008, Phys. Rev. D, 78, 123523
- Peebles, P. J. E. 1969, ApJ, 155, 393
- Perlmutter, S., Aldering, G., Goldhaber, G., et al. 1999, ApJ, 517, 565
- Reyes, R., Mandelbaum, R., Seljak, U., et al. 2010, Nature, 464, 256
- Riess, A. G., Filippenko, A. V., Challis, P., et al. 1998, AJ, 116, 1009
- Schmidt, F., Vikhlinin, A., & Hu, W. 2009, Phys. Rev. D, 80, 083505
- Schmidt, F. 2010, Phys. Rev. D, 81, 103002
- Sotiriou, T. P., & Faraoni, V. 2010, Reviews of Modern Physics, 82, 451
- Starobinsky, A. A. 1980, Physics Letters B, 91, 99
- Steinmetz, M., & Bartelmann, M. 1995, MNRAS, 272, 570
- Wall, J. V., & Jenkins, C. R. 2003, Practical statistics for astronomers, (Cambridge: New-York)
- Wojtak, R., Hansen, S. H., & Hjorth, J. 2011, Nature, 477, 567
- Zhao, G.-B., Li, B., & Koyama, K. 2011, Phys. Rev. D, 83, 044007

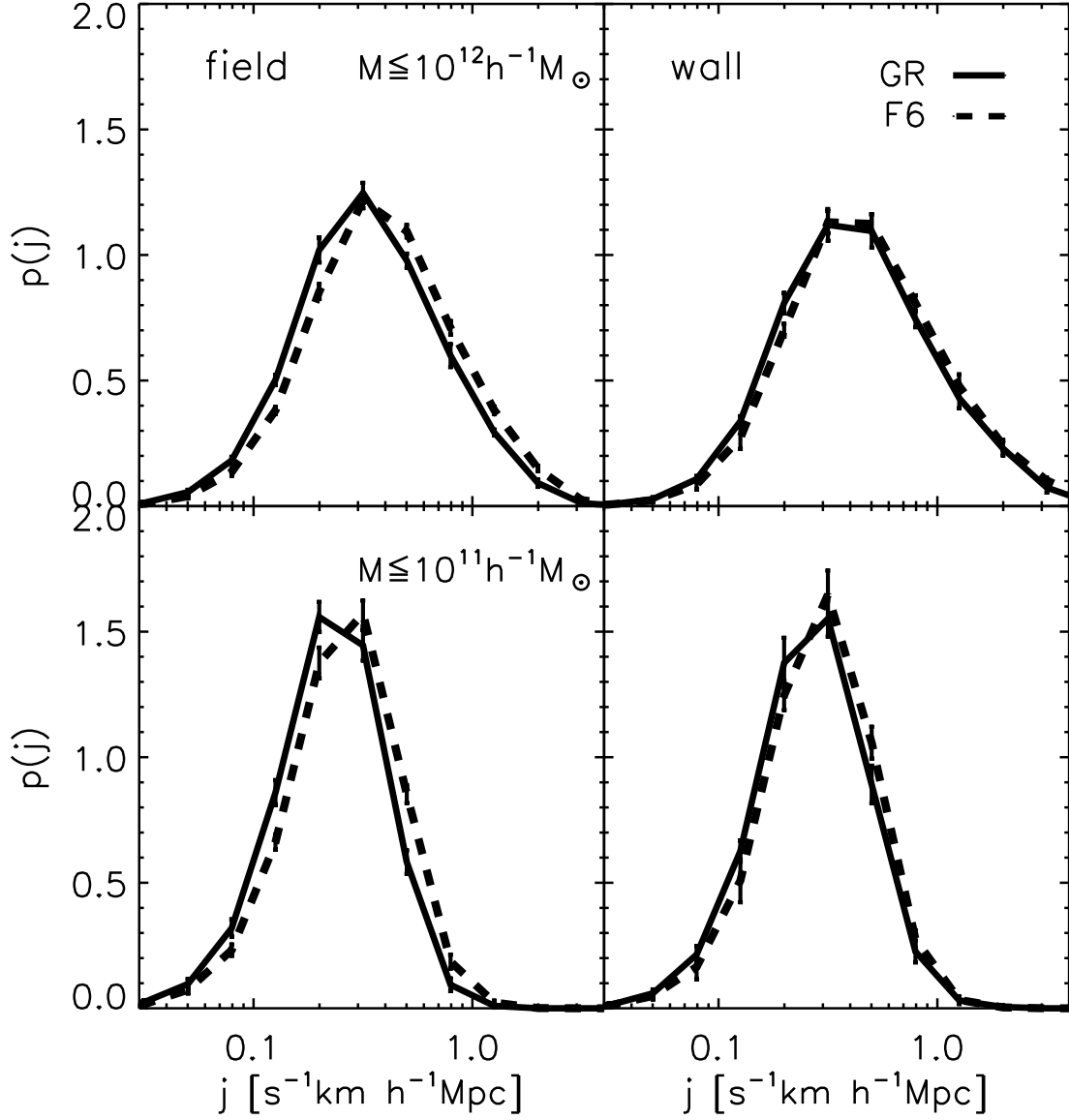


Fig. 1.— Probability density distributions of the specific angular momentum of the field and wall galactic halos in the left and right panels, respectively. The top and bottom panels correspond to the case that the galactic halos with masses of $M \leq 10^{12} h^{-1} M_{\odot}$ and of $M \leq 10^{11} h^{-1} M_{\odot}$, respectively. In each panel, the solid and the dashed lines correspond to the standard GR+ Λ CDM and F6 case, respectively. The errors are obtained using eight Jackknife resamples.

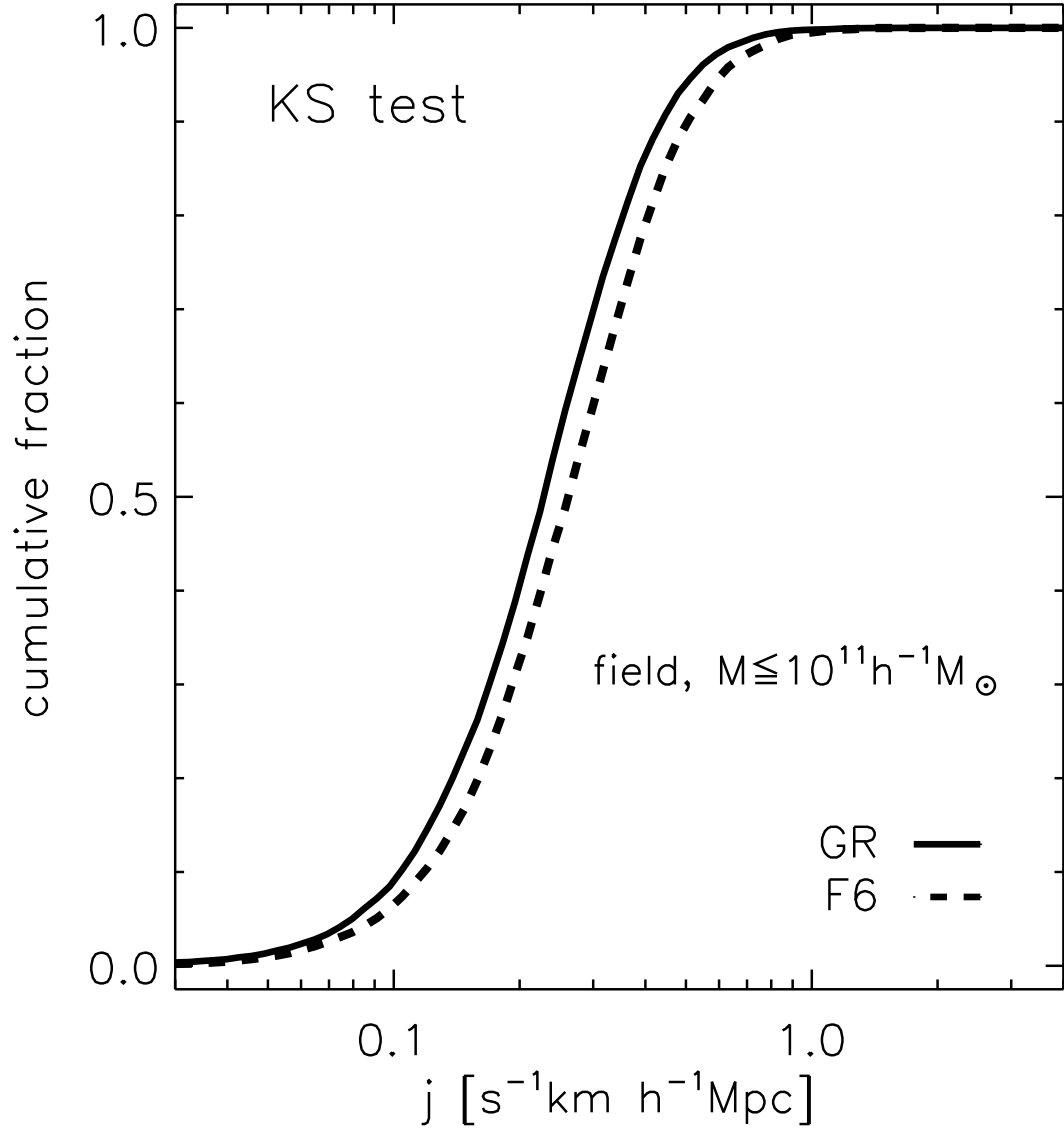


Fig. 2.— K-S test cumulative fractional plot of the specific angular momentum of the field galactic halos for the two models.

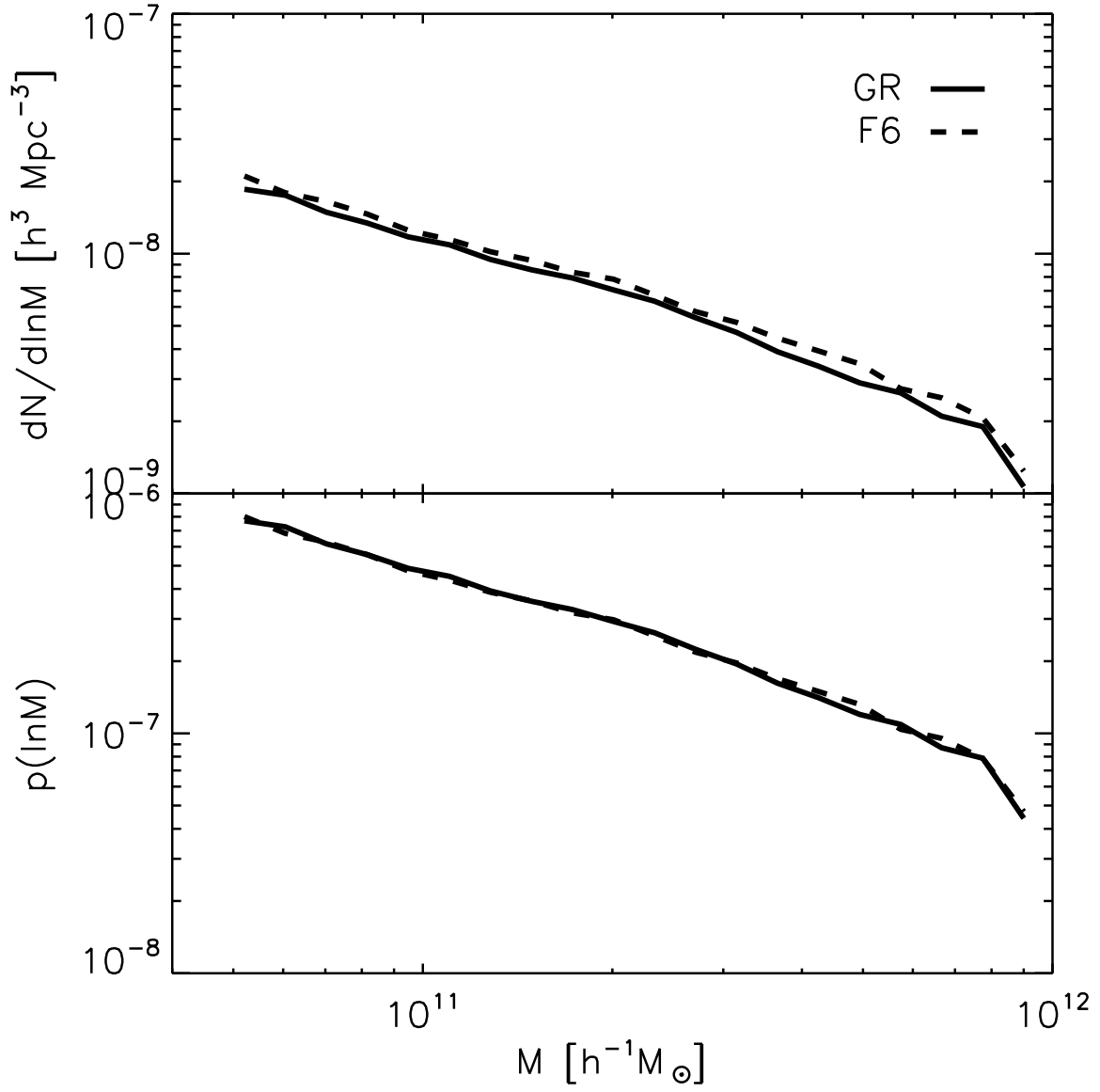


Fig. 3.— Number and probability densities of the galactic halos as a function of their logarithmic mass in the top and bottom panel, respectively.

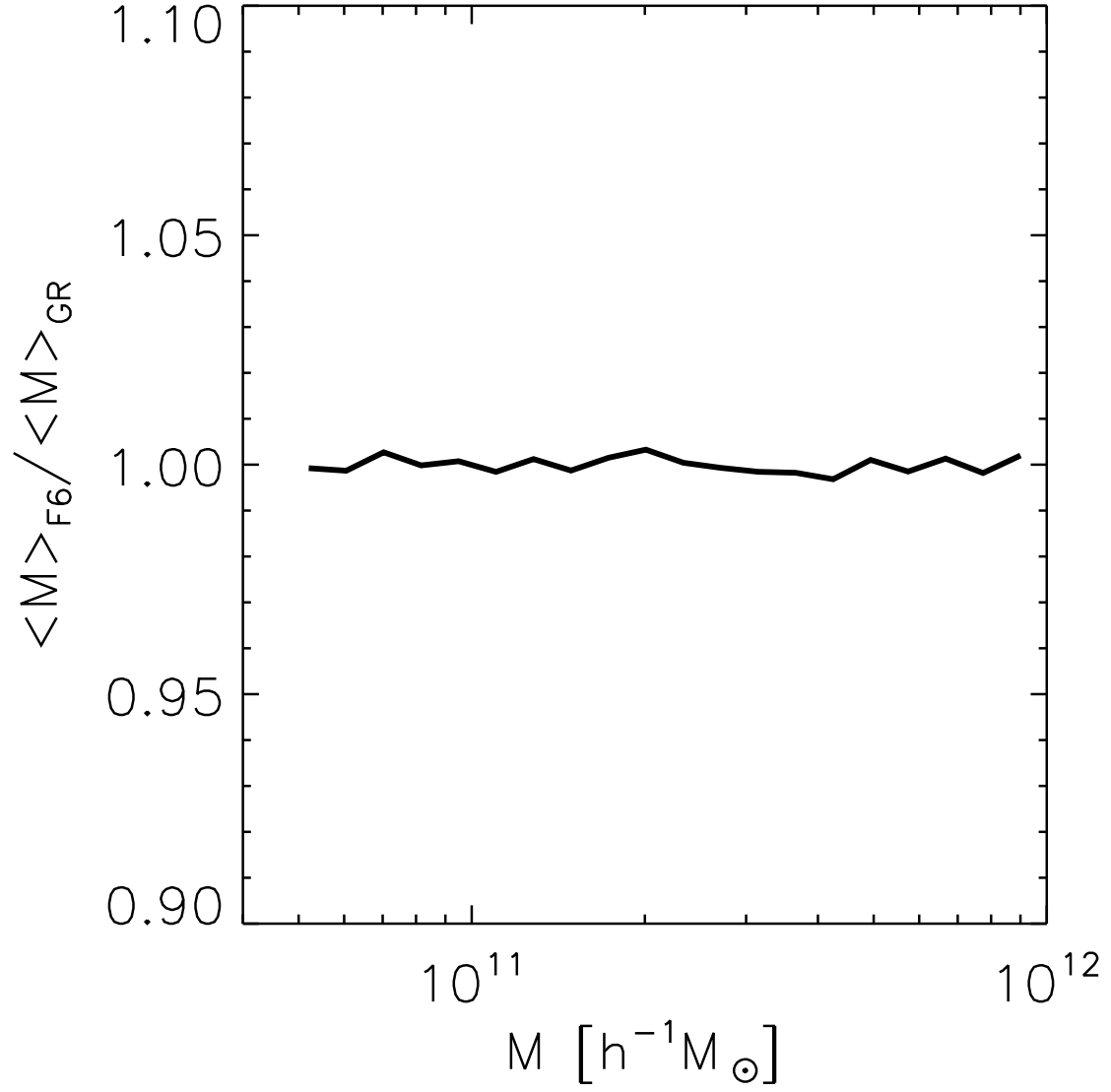


Fig. 4.— Ratio of the mean mass of the galactic halos in the F6 model to that in the GR model.

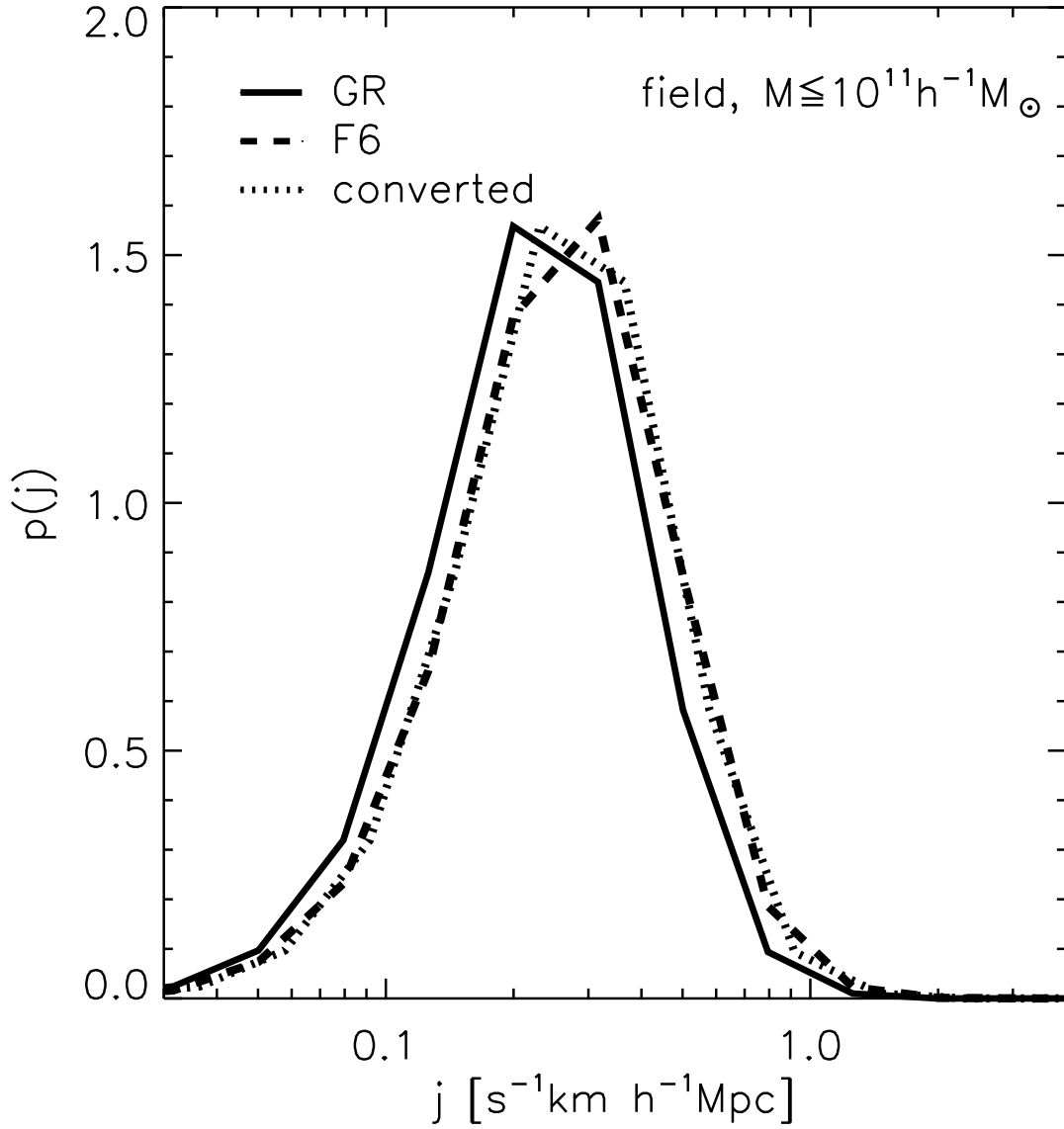


Fig. 5.— Same as the top-left panel of Figure 1 but plotting also the converted probability density distribution of j (dotted line) obtained by multiplying the values of j for the GR case by a factor of $(4/3)^{1/2}$.

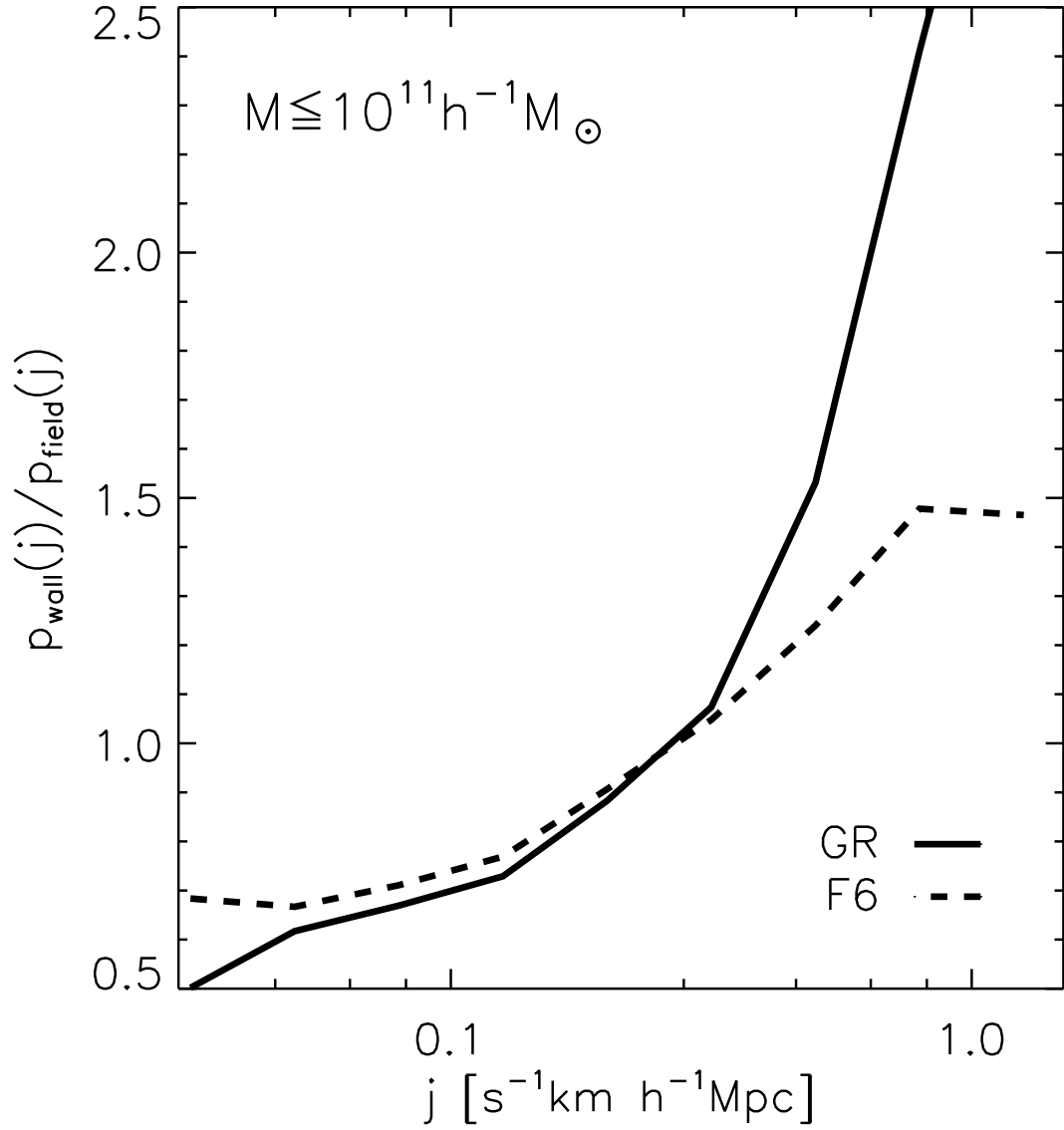


Fig. 6.— Ratio of the probability density of the field galactic halos to that of the wall galactic halos for the two models.

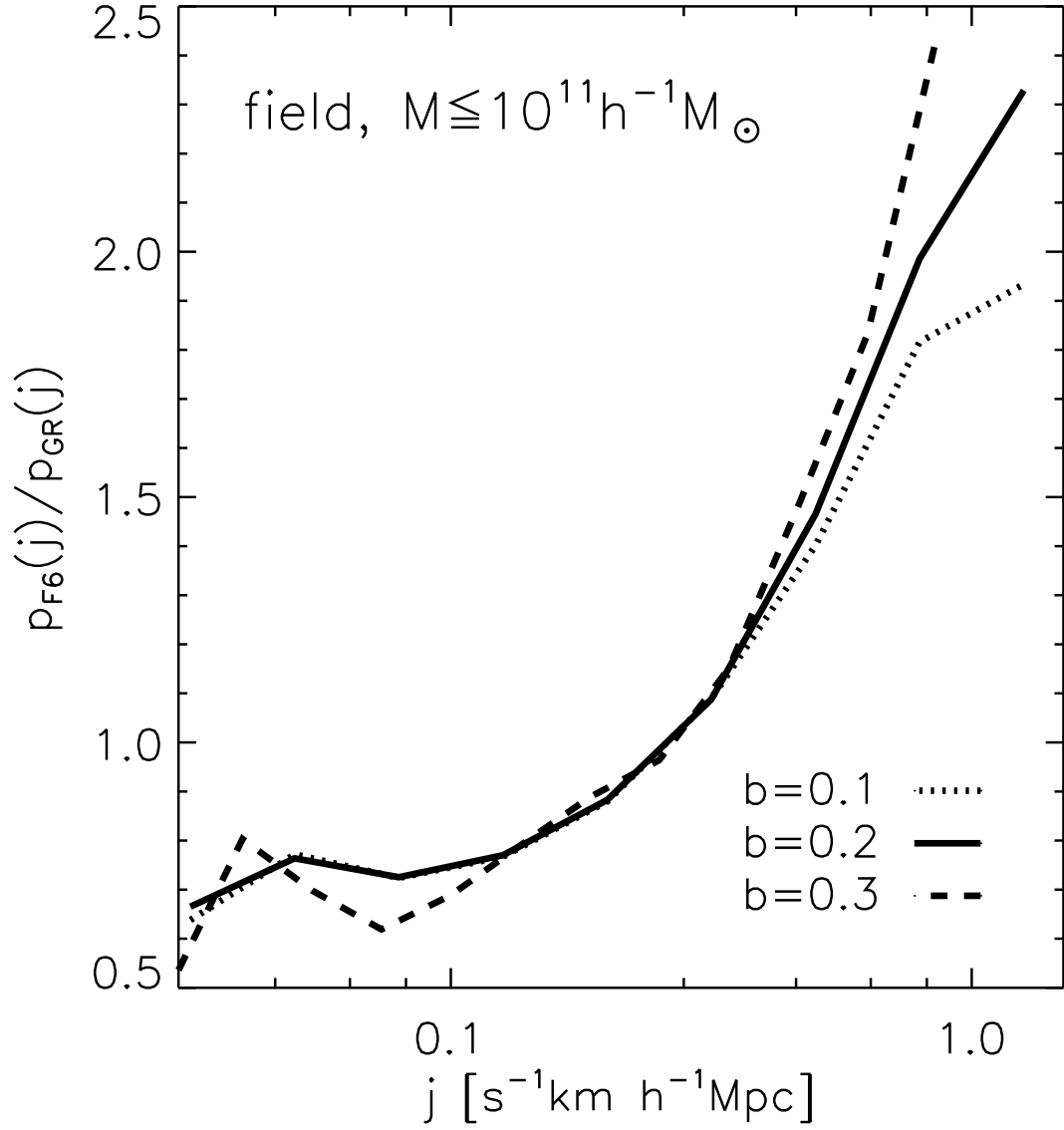


Fig. 7.— Ratio of the probability density of the field galactic halos in the GR model to that in the F6 model for the three different cases of the linkage length parameter.

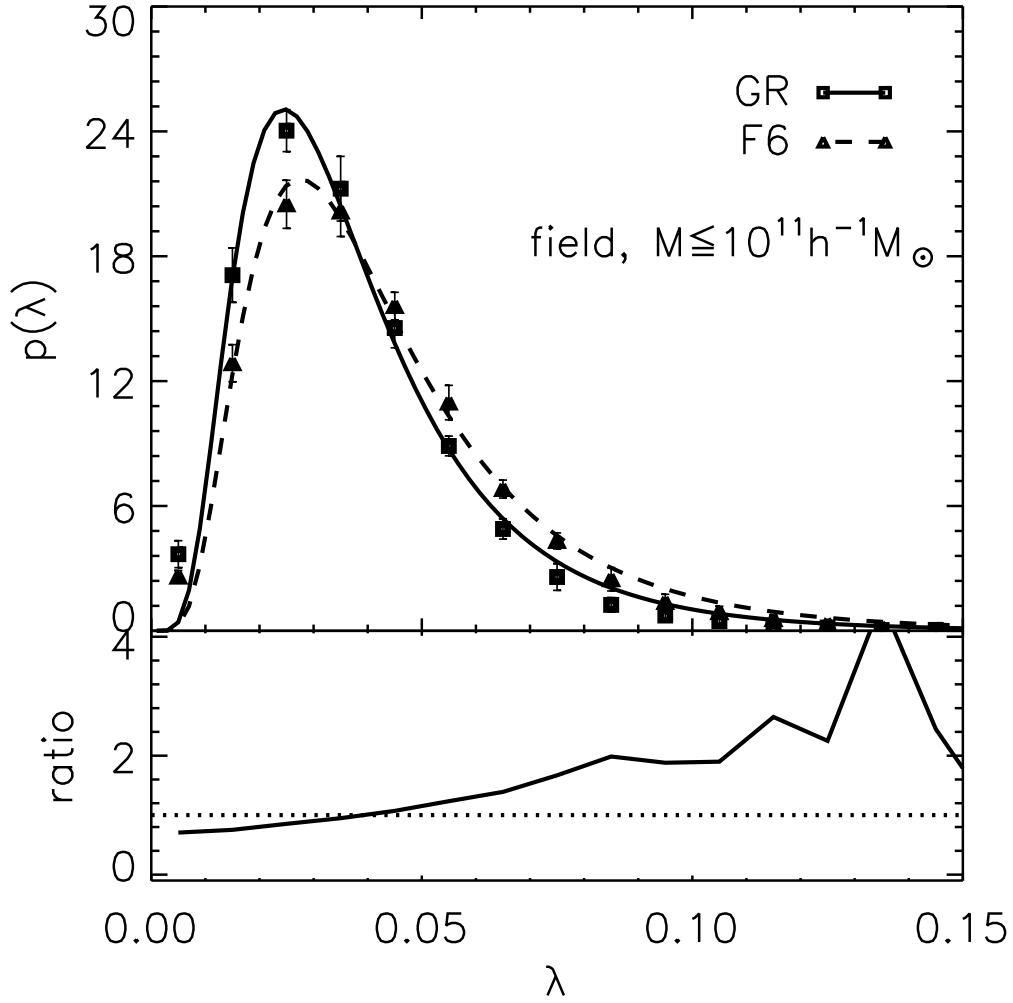


Fig. 8.— (Top panel): Probability density distributions of the spin parameter of the field galactic halos for the GR and F6 case as square and triangle dots, respectively. The solid and dashed lines correspond to the best-fit log-normal distributions for the GR and F6 case, respectively. (Bottom panel): Ratio of $p(\lambda)$ for the F6 case to that for the GR case. The dotted line corresponds to the flat case.

Table 1. model, # of the well-resolved halos with $N_p \geq 100$ (N_{total}), the mean halo separation, # of the field galactic halos for the two different mass thresholds

model	N_{total}	$\bar{\ell}$ [$h^{-1}\text{Mpc}$]	$N_{\text{field,I}}$ ($M \leq 10^{12} h^{-1} M_{\odot}$)	$N_{\text{field,II}}$ ($M \leq 10^{11} h^{-1} M_{\odot}$)
GR	43396	2.846	24114	11252
F6	47517	2.761	26297	12299

Table 2. model, two best-fit values of the spin parameter distribution

model	λ_0	σ_λ
GR	0.033	0.556
F6	0.038	0.569